

# Stabilizing period-doubled density waves by spin-orbit coupling in Bose-Einstein condensates in optical lattices

Chenhui Wang and Yongping Zhang\*

*Institute for Quantum Science and Technology, Department of Physics, Shanghai University, Shanghai 200444, China*

In atomic Bose-Einstein condensates in optical lattices, mean-field energy can support the existence of period-doubled density waves, which are similar to Bloch waves but have the double periodicity of the underlying lattice potentials. However, they are dynamically unstable. Here, we propose to use the spin-orbit coupling to stabilize the period-doubled density waves. The stabilization mechanism is revealed to relate to interaction-induced spontaneous symmetry breaking of the spin-flip parity symmetry.

## I. INTRODUCTION

Atomic Bose-Einstein condensates (BECs) loaded into optical lattices (OLs) have been important quantum many-body platforms for exploring fundamental physics, emphasizing the interplay between atomic interactions and periodic potentials. [1–8]. In the mean-field frame, atomic contact interactions become the mean-field nonlinearity [9]. The combination of the mean-field energy and OLs gives rise to the nonlinear Bloch band-gap spectrum with associated nonlinear Bloch waves (NBWs) which have the same periodicity as OLs. The investigations into NBWs and nonlinear spectrum attract great research attention [10–13]. Elementary excitation of the ground-state NBW also features a Bloch band-gap structure, with the lowest band being relevant to sound excitation [14]. The sound velocity has been measured to reflect superfluid density [15, 16]. The mean-field energy may bring dynamical and energetic instabilities to NBWs [3, 12, 17–19]. Both the instabilities have been experimentally observed to break down the lattice superfluidity of BECs [20, 21]. The motions induced by an accelerating force have shown the asymmetric Landau-Zener behavior between the transition from the lowest to the first nonlinear Bloch bands and the reversed transition [22]. When the mean-field energy dominates over OLs, a loop structure appears to adhere to a certain nonlinear Bloch band [19]. Bloch waves in the loop do not have linear analogues [23]. The motions along the looped nonlinear Bloch band result in nonlinear Landau-Zener tunneling [4]. Its transition probability does not obey the conventional Landau-Zener formulae, and the transition happens even in the adiabatic limit of the accelerating force [24]. The loop-induced nonlinear Landau-Zener tunneling has been observed and explored in experiments [25, 26].

The mean-field energy can also support period-doubled or even multiple-period density waves in BECs in OLs [5, 27–29]. Akin to NBWs, the period-doubled density waves (PDDWs) are spatially extensive and periodic but have a periodicity that is twice that of OLs. The PDDW patterns may appear even in a superfluid Fermi gas [30].

Their existence is a complete nonlinear phenomenon. Without the mean-field energy, these states can not exist. These density-wave patterns may be considered as periodic trains of solitons [28]. The relation between them and the NBWs inside the loop structure has been discussed [27]. The construction of the PDDWs from two different linear Bloch waves with equal energy has been systematically studied [29]. It has been found that the PDDWs are always dynamically unstable [27, 29], which challenges experimentally direct observations. How to stabilize them immediately becomes an important problem. In Ref. [31], Maluckov *et al.* reveal that the long-range dipole-dipole interactions can be used to stabilize the PDDWs and consider such stable patterns as a kind of supersolids since they spontaneously break the translation symmetry of OLs. So far, the long-range interactions are the only reported approach for stabilization.

In this paper, we provide an alternative approach to stabilize the PDDWs. Our approach lies in spin-orbit coupling (SOC) and, therefore, does not need to engineer interactions. As an intrinsic interaction between the motion and spin of a particle, SOC in solid-state materials plays an essential role in many interesting physical phenomena and applications, such as the spin Hall effect [32, 33]. Artificial SOC has been successfully realized in BECs [34–41], providing an experimentally accessible platform for exploring exotic superfluidity [42–47] and elementary excitations [37, 38]. Especially, experimentally loading the spin-orbit-coupled BECs (SOC-BECs) into OLs [39, 48] greatly stimulates research efforts on the rich emergent physics stemming from the interplay between the SOC and lattice effects [49–59]. One of the outstanding features in SOC-BECs with OLs is that the lowest nonlinear Bloch band may be flat [60]. A family of Wannier solitons can be bifurcated from this flat band [61]. An unconventional spin dynamics can be induced by the SOC in a random OL [62, 63].

We study the PDDWs in SOC-BECs loaded into OLs. Without the SOC, the PDDWs are always dynamically unstable. The PDDWs have a negative effective mass. It is known that the state with negative effective mass is unstable in the presence of repulsive contact interactions. The negative effective mass of the PDDWs is protected by the parity symmetry. The SOC leads to the parity being joined with the spin-flip. The contact interactions

\* yongping11@t.shu.edu.cn

can spontaneously break the joint symmetry by destroying its spin-flip part. The spontaneous symmetry breaking can change the effective mass of the PDDWs from originally negative to positive. Finally, the PDDWs may achieve a positive effective mass, which provides a possibility of stabilization in the presence of repulsive contact interactions.

This paper is organized as follows. In Sec. II, we present the theoretical frame for the study on SOC-BECs with OLs. It includes the system of the SOC-BEC in OLs, the PDDW solutions, and the linear stability analysis by the Bogoliubov-de Gennes equation. In Sec. III, we reveal the spontaneous symmetry breaking of the PDDWs. In Sec. IV, the stabilization mechanism for the PDDWs is addressed. We systematically check their stability in the full parameter space. Finally, the conclusion is provided in Sec. V.

## II. MODEL

Our system is based on the experimentally realizable SOC-BECs in OLs in the Ref. [39]. Two hyperfine states of the elongated  $^{87}\text{Rb}$  BEC are coupled by two oppositely propagating Raman lasers with the wave number  $k_R$ . The two-photon coupling transfers the recoil momentum  $2\hbar k_R$  to the BEC, generating the SOC,  $p_x\sigma_z$ , with the SOC strength  $\hbar k_R/m$ ,  $m$  the mass of atom,  $p_x$  the momentum of atoms along the propagation direction of lasers, and  $\sigma_z$  the standard Pauli matrix [46, 47]. The implemented SOC-BEC is loaded into an OL by adiabatically ramping up the lattice lasers with the wave number  $k_L$  along the same direction as the Raman lasers. Such the SOC-BEC in the OLs can be described by the dimensionless Gross-Pitaevskii equation (GPE) for the spinor  $\Psi$ ,

$$i\partial_t\Psi = H_{SOC}\Psi + g(\Psi^\dagger\Psi)\Psi, \quad (1)$$

where

$$H_{SOC} = -\frac{1}{2}\partial_x^2 - i\gamma\partial_x\sigma_z + \frac{\Omega}{2}\sigma_x + V_0\sin^2(x), \quad (2)$$

is the single-particle spin-orbit-coupled Hamiltonian,  $\gamma = k_R/k_L$  is the SOC strength,  $\Omega$  is the Rabi frequency, and  $V_0$  is the amplitude of the OL [39]. The units of energy and length are chosen as  $2E_L$  and  $1/k_L$ , respectively, where  $E_L = \hbar^2 k_L^2/2m$  is the recoil energy of the lattice lasers. In the GPE, the last term describes the contact interactions. In  $^{87}\text{Rb}$  BEC experiments, the inter- and intra-component interactions are almost same [39]. Therefore, we have assumed the repulsive interactions having the same coefficient,  $g = 2Nm\omega_r a_0/\hbar\pi k_L$ , with  $N$  being the average number of atoms inside a unit cell of OLs,  $a_0$  being spin-independent scattering length and  $\omega_r$  being the trap frequency along the transverse directions. The dimensionless order parameter  $\Psi$  satisfies the

normalization condition,

$$\frac{1}{S\pi}\int_0^{S\pi}\Psi^\dagger\Psi dx = 1, \quad (3)$$

with  $S = 1$  for the NBWs and  $S = 2$  for the PDDWs, since the size of a unit cell for these two solutions is  $S\pi$  and the normalization is performed over a unit cell.

In the detailed calculations, we consider the typical experimental parameters [39]:  $k_R = 5.63\mu\text{m}^{-1}$  and  $k_L = 2.88\mu\text{m}^{-1}$ . Consequently, the dimensionless SOC strength becomes  $\gamma = k_R/k_L = 1.95$ . The Rabi frequency  $\Omega$  and the amplitude of the OL  $V_0$  are free parameters that can be tuned by changing the intensity of the Raman and lattice beams, respectively. We set  $V_0 = 2$  in the following concrete calculations.

The periodic solutions, including NBWs and PDDWs, are stationary [29, 31],

$$\Psi(x, t) = e^{-i\mu t}\mathbf{u}(x), \quad (4)$$

where  $\mu$  is the chemical potential, and  $\mathbf{u}(x) = [u_1(x), u_2(x)]^T$  is a periodic function satisfying  $\mathbf{u}(x + S\pi) = \mathbf{u}(x)$ . For  $S = 2$ , the solutions become the PDDWs. For a comparison, we also study the corresponding NBW solutions in the case of  $S = 1$ . It is noticed that the corresponding NBWs have a zero quasi-momentum. The periodic functions obey the stationary GPE,

$$\mu\mathbf{u} = H_{SOC}\mathbf{u} + g(|u_1|^2 + |u_2|^2)\mathbf{u}. \quad (5)$$

They are expanded on a plane-wave basis considering their periodicity,

$$\mathbf{u} = \sum_{n=-L}^L \begin{pmatrix} a_n \\ b_n \end{pmatrix} e^{i\frac{2}{S}nx}, \quad (6)$$

where  $L$  is the cut-off of plane-wave modes. The plane-wave coefficients  $a_n$  and  $b_n$  satisfy the normalization condition  $\sum_{n=-L}^L (|a_n|^2 + |b_n|^2) = 1$  according to the Eq. (3). We numerically solve the stationary GPE together with the normalization condition by the standard Newton relaxation method to obtain  $a_n, b_n$  and  $\mu$  for the PDDWs and NBWs. Once the solutions are known, we calculate their spin polarization  $\langle\sigma_z\rangle$ , which is defined as

$$\begin{aligned} \langle\sigma_z\rangle &= \langle\mathbf{u}|\sigma_z|\mathbf{u}\rangle = \frac{1}{S\pi}\int_0^{S\pi} (|u_1|^2 - |u_2|^2)dx \\ &= \sum_{n=-L}^L (|a_n|^2 - |b_n|^2). \end{aligned} \quad (7)$$

The dynamical stability of the PDDWs and NBWs is an important issue and is relevant to their experimental realizations [17, 21]. We study the stability by the linear stability analysis and assume that the solutions are perturbed by small perturbations,

$$\delta u_j = U_j(x)\exp(iqx - i\omega t) + V_j^*(x)\exp(-iqx + i\omega^*t), \quad (8)$$

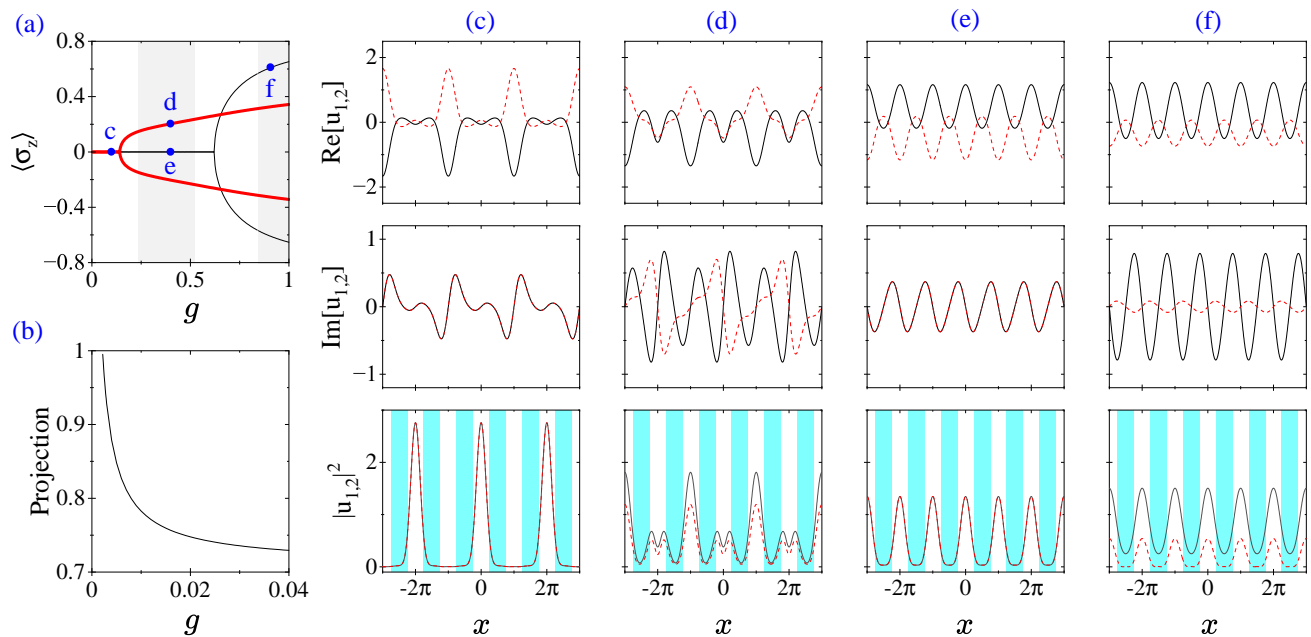


FIG. 1. Existence and spontaneous symmetry breaking of the PDDWs and NBWs. (a) The spin polarization  $\langle \sigma_z \rangle$  of the PDDWs (the red-thick line) and NBWs (the black-thin line) shows a bifurcation relevant to the spontaneous symmetry breaking. The states in the shadow regions are dynamically stable, and other states are dynamically unstable. The profiles of states represented by labeled points are shown in (c)-(f). (c) and (d) are for the PDDWs, and (e) and (f) correspond to the NBWs. The upper and middle panels show the real and imaginary parts of the wave function, respectively. The lower panel describes the density distributions  $|\mathbf{u}(x)|^2$ . The black solid lines are for  $u_1$ , and the red-dash lines are for  $u_2$ . The blue shadow areas represent the regions of  $\sin^2(x) > 1/2$ . (b) The projection of the PDDWs to the associated linear Bloch wave. There is a bound value  $g_b \sim 3 \times 10^{-3}$ . When  $g < g_b$ , the PDDWs can not exist. In all plots, dimensionless parameters are  $V_0 = 2, \gamma = 1.95$ , and  $\Omega = 5$ .

where  $j = 1, 2$ ,  $U_j$  and  $V_j$  represent perturbation amplitudes, and  $q$  and  $\omega$  are the quasimomentum and energy of perturbations, respectively. Substituting the perturbed solutions  $e^{-i\mu t}[\mathbf{u}(x) + \delta\mathbf{u}(x, t)]$  with  $\delta\mathbf{u}(x, t) = [\delta u_1, \delta u_2]^T$  into Eq. (1) and keeping linear terms with respect to the perturbation amplitudes, we obtain the following Bogoliubov-de Gennes (BdG) equation,

$$\mathcal{H}_{BdG}\varphi = \omega\varphi. \quad (9)$$

Here,  $\varphi = (U_1, U_2, V_1, V_2)^T$ , and the BdG Hamiltonian,

$$\mathcal{H}_{BdG} = \begin{pmatrix} \mathcal{A}(q) & \mathcal{B} \\ -\mathcal{B}^* & -\mathcal{A}^*(-q) \end{pmatrix}, \quad (10)$$

with

$$\mathcal{A}(q) = \begin{pmatrix} \mathcal{L}_1(q) & gu_1u_2^* + \Omega/2 \\ gu_1^*u_2 + \Omega/2 & \mathcal{L}_2(q) \end{pmatrix},$$

$$\mathcal{B} = g \begin{pmatrix} u_1^2 & u_1u_2 \\ u_1u_2 & u_2^2 \end{pmatrix},$$

and

$$\mathcal{L}_j(q) = -\frac{1}{2}(iq + \partial_x)^2 + (-1)^j i\gamma(iq + \partial_x) - \mu$$

$$+ V_0 \sin^2(x) + g(2|u_j|^2 + |u_{3-j}|^2).$$

The outstanding feature of the BdG Hamiltonian is that it is non-Hermitian, which allows the existence of imaginary excitation modes in  $\omega$ . In the presence of imaginary modes in  $\omega$ , the perturbations shall grow exponentially as indicated from Eq. (8). Such dynamical growth of the perturbations shall destroy the corresponding BEC states, generating dynamical instability. For the PDDWs and NBWs, the BdG Hamiltonian is periodic with the period of  $S\pi$ . We employ the plane-wave basis for  $\varphi$ , i.e.,  $\varphi = \sum_{n=-L}^L \varphi_n e^{i2nx/S}$ , with the superposition coefficients  $\varphi_n$ . In the plane-wave basis, the BdG Hamiltonian can be directly diagonalized, and the excitation spectrum  $\omega$  can be obtained. Whether there includes imaginary modes or not is used to judge the dynamical stability of the PDDWs and NBWs.

### III. SPONTANEOUS SYMMETRY BREAKING OF PDDW

Applying the theoretical frame described in the previous section, we search for the PDDWs ( $S = 2$ ) and the relevant NBWs ( $S = 1$ ) in the lowest band. Their existence is demonstrated in Fig.1. For  $g = 0.1$ , profiles of the PDDW are shown in Fig.1(c). The real and imaginary parts of  $u_j$  are demonstrated in the upper and

middle panels, respectively. From these two panels, we know that the real part satisfies  $\text{Re}[u_1(x)] = -\text{Re}[u_2(x)]$  and has an even parity, and the imaginary part satisfies  $\text{Im}[u_1(x)] = \text{Im}[u_2(x)]$  and has an odd parity. The single-particle spin-orbit-coupled Hamiltonian  $H_{SOC}$  has a group of symmetries  $\{1, \hat{\alpha}_1, \hat{\alpha}_2, \hat{\alpha}_3\}$ , where

$$\hat{\alpha}_1 = \mathcal{P}\mathcal{K}, \quad \hat{\alpha}_2 = \mathcal{P}\sigma_x, \quad \hat{\alpha}_3 = \mathcal{K}\sigma_x, \quad (11)$$

with  $\mathcal{P}$  being the parity operator and  $\mathcal{K}$  the complex conjugate operator, i.e.,  $[\hat{\alpha}_j, H_{SOC}] = 0$ . The PDDW in Fig.1(c) obeys all these symmetries and is their eigenstate. The eigenvalue equations are  $\hat{\alpha}_1\mathbf{u}(x) = \mathbf{u}(x)$  with the eigen value  $+1$  and  $\hat{\alpha}_3\mathbf{u}(x) = -\mathbf{u}(x)$  with the eigen value  $-1$ . From these eigenvalue equations, we know that the real part of  $\mathbf{u}(x)$  has an even parity and the imaginary part has an odd parity, and the relationship  $\text{Re}[u_1(x)] = -\text{Re}[u_2(x)]$  and  $\text{Im}[u_1(x)] = \text{Im}[u_2(x)]$  is natural. The density distributions  $|\mathbf{u}(x)|^2$  are shown in the lower panel in Fig.1(c). The spin-flip symmetries  $\hat{\alpha}_2$  and  $\hat{\alpha}_3$  give rise to  $|u_1(x)|^2 = |u_2(x)|^2$ . The densities have the vanishing occupation of neighbor sites of the OL, which is the signature of the PDDWs. Due to  $|u_1(x)|^2 = |u_2(x)|^2$ , it is easy to identify  $\langle\sigma_z\rangle = 0$ , which is demonstrated in Fig.1(a).

We emphasize that the family of the PDDW shown in Fig.1(c) bifurcates from the associated linear Bloch wave. We first find the associated linear Bloch wave (which is the Bloch wave with the zero quasimomentum in the lowest band) in the absence of nonlinearity  $g = 0$ . Then, we calculate the projection, which is defined as the overlap between the associated linear Bloch wave and the PDDW. The projection is demonstrated in Fig.1(b) as a function of the nonlinear coefficient  $g$ . As  $g$  decreases towards 0, the projection goes to 1, indicating that the family indeed bifurcates from the linear Bloch wave. There is a bound value for the coefficient,  $g_b \sim 3 \times 10^{-3}$ . If  $g < g_b$ , the PDDW can not exist. This confirms that the PDDWs are a pure nonlinear phenomenon and do not have a linear analog.

When the interaction coefficient  $g$  is small, the PDDWs follow all symmetries of the spin-orbit coupling, the most important consequence of which is their zero spin polarization  $\langle\sigma_z\rangle = 0$ . We find that a large interaction coefficient can make the PDDWs to spontaneously break the spin-flip symmetries  $\hat{\alpha}_2$  and  $\hat{\alpha}_3$ . Fig.1(a) illustrates the spontaneous symmetry breaking [see the red-thick line]. When the coefficient  $g$  is beyond a critical value  $g_c$ , i.e.,  $g > g_c$ , the PDDWs bifurcate into two branches. The spin polarization of the two branches is not zero and has opposite signs. A typical PDDW in one of the two branches [labeled by “d” in Fig.1(a)] is depicted in Fig.1(d). The PDDW still keeps the  $\hat{\alpha}_1$  symmetry and satisfies  $\hat{\alpha}_1\mathbf{u}(x) = \mathbf{u}(x)$  with the eigen value being  $+1$ . Therefore, the parity of the real (imaginary) part is even (odd) [see the upper and middle panels in Fig.1(d)]. This state does not obey the spin-flip symmetries  $\hat{\alpha}_2$  and  $\hat{\alpha}_3$ . As a result,  $|u_1(x)|^2 \neq |u_2(x)|^2$ . The density distributions demonstrated in the lower panel in Fig.1(d) clearly

show the mismatch of two-component densities. The interesting feature of this symmetry-breaking state is that all sites have occupations, and populations in neighbor sites are different in order to realize the PDDWs. This state  $\mathbf{u}(x)$  spontaneously breaks the spin-flip symmetries, and therefore, it is not their eigenstate. Actually,  $\hat{\alpha}_2\mathbf{u}(x)$  (which is the same as  $\hat{\alpha}_3\mathbf{u}(x)$  considering  $\hat{\alpha}_3 = \hat{\alpha}_1\hat{\alpha}_2$ ) turns to be the state in the other branch shown in Fig.1(a). The spin polarization in the other branch becomes  $\langle\hat{\alpha}_2\mathbf{u}(x)|\sigma_z|\hat{\alpha}_2\mathbf{u}(x)\rangle = \langle\mathcal{P}\mathbf{u}(x)|\sigma_x\sigma_z\sigma_x|\mathcal{P}\mathbf{u}(x)\rangle = -\langle\mathbf{u}(x)|\sigma_z|\mathbf{u}(x)\rangle$ . Therefore, the two branches have the same spin polarization but with opposite signs.

We find that the relevant NBWs have a similar behavior of spontaneous symmetry breaking as the PDDWs. The existence of the NBWs is shown by the black-thin line in Fig.1(a). When  $g$  is not large, the NBWs follow the spin-flip symmetries and feature  $\langle\sigma_z\rangle = 0$ . A typical profile of such NBWs is shown in Fig.1(e). The symmetries  $\hat{\alpha}_i$  make the real (imaginary) part of the wave function to be even (odd) and generate  $\text{Re}[u_1(x)] = -\text{Re}[u_2(x)]$  and  $\text{Im}[u_1(x)] = \text{Im}[u_2(x)]$ . Different from the PDDW in Fig.1(c), the densities  $|u_1(x)|^2 = |u_2(x)|^2$  distribute in every site as shown in the lower panel of Fig.1(e). When  $g$  is large, the NBWs spontaneously break the spin-flip symmetries  $\hat{\alpha}_2$  and  $\hat{\alpha}_3$  and feature two branches with opposite  $\langle\sigma_z\rangle$  [see Fig.1(a)]. A profile of the NBW in one of the branches is demonstrated in Fig.1(f). The real and imaginary parts in the upper and middle panels show that the NBW still follows the  $\hat{\alpha}_1$  symmetry. The densities  $|u_1(x)|^2 \neq |u_2(x)|^2$  are shown in the lower panel.

#### IV. STABILIZING PDDW

We first explain the reason that the PDDWs without the SOC are always dynamically unstable. The typical linear Hamiltonian is  $H_{lin} = -\partial_x^2/2 + V_0 \sin^2(x)$ , including the kinetic energy and an OL. The Hamiltonian features Bloch band-gap spectrum  $E_{nk}$  with associated Bloch waves. Here,  $n$  labels the  $n$ -th band, and  $k$  is the quasimomentum. Due to the parity symmetry  $\mathcal{P}$  of  $H_{lin}$ , we have  $E_{nk} = E_{n(-k)}$ . Therefore,  $k = 0$  is a high symmetric point. The important consequence is  $\partial_k E_{nk} = 0$  at the high symmetric point. So at  $k = 0$ ,  $E_{nk}$  must be an extreme value due to the parity symmetry. If it is a local minimum, the effective mass of the Bloch wave at  $k = 0$  is positive,  $m_{eff} \propto 1/\partial_k^2 E_{nk} > 0$ . If it is a local maximum, the effective mass of the Bloch wave at  $k = 0$  is negative. Now, let’s include the contact interactions and consider the PDDWs. Similar to Bloch waves, the generalized PDDWs are defined as  $e^{ikx}u_{pd}(x)$  with the periodic functions satisfying  $u_{pd}(x + 2\pi) = u_{pd}(x)$ . They always follow the parity symmetry of  $H_{lin}$ . Then the nonlinear energy of the PDDW at  $k = 0$  is an extreme value. It has been shown by numerical calculations that the PDDW at  $k = 0$  always belongs to a local maximum [27–29]. Therefore, the PDDW at  $k = 0$  al-

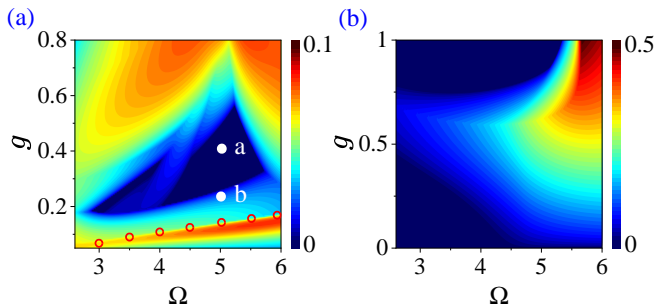


FIG. 2. The stability regions of the PDDWs (a) and the relevant NBWs (b) in the parameter space  $(\Omega, g)$ . The color scale represents the maximum of the imaginary part of  $\omega$ ,  $\text{Max}(\text{Im}[\omega])$ . Stable PDDWs and NBWs having  $\text{Max}(\text{Im}[\omega]) = 0$  are in the dark-colored regions. The open circles represent the critical values  $g_c$  of the nonlinearity beyond which the PDDWs break the spin-flip parity symmetry. The two white-solid circles labeled by “a” and “b” represent the stable and unstable PDDWs, respectively, whose Bogoliubov spectrum and dynamical evolutions shall be demonstrated in Fig. 3 and Fig. 4. Other parameters are  $\gamma = 1.95$  and  $V_0 = 2$ .

ways takes the negative effective mass. It is known that the state with the negative effective mass is dynamically unstable in the presence of the repulsive contact interactions [3, 10, 17, 21, 60, 64–66]. Such the instability of the state with the negative effective mass can be understood as the interactions that it effectively feels are attractive. Finally, we conclude that the PDDW at  $k = 0$  is dynamically unstable. We emphasize that it is the parity symmetry of  $H_{lin}$  that conserves the sign of effective mass of the PDDW at  $k = 0$  for all different parameters.

The PDDW we consider in Eq.(4) belongs to the PDDW at  $k = 0$ . In the presence of the SOC, the parity must be associated with the spin. Indeed, the  $H_{SOC}$  respects the spin-flip parity symmetry,  $\hat{\alpha}_2 = \mathcal{P}\sigma_x$ . The PDDWs also obey this symmetry when the interaction coefficient  $g$  is not dominant. The signature of the symmetry is  $\langle \sigma_z \rangle = 0$ . This symmetry makes the PDDW at  $k = 0$  to be an extreme value state. Similar to the case without the SOC, the PDDW at  $k = 0$  is a local maximum state. It is straightforward to expect that the PDDWs are dynamically unstable. We systematically check their instability by the calculation of the BdG equation. The results agree with the prediction that all PDDWs having the spin-flip parity symmetry are unstable.

The spin-flip parity symmetry,  $\hat{\alpha}_2 = \mathcal{P}\sigma_x$ , originating from the SOC, offers a possible spin channel for its breaking down. When the interaction coefficient  $g$  is dominant, the PDDWs spontaneously break the  $\hat{\alpha}_2$  symmetry by not following its spin part  $\sigma_x$ . Because of the symmetry breaking, the PDDWs  $\mathbf{u}(x)$  and  $\hat{\alpha}_2\mathbf{u}(x)$  are no longer the same state. These two independent states are not the extreme value states anymore, therefore lost the guarantee that their effective mass should be negative. Once they get the positive effective mass, they might be

stable considering the repulsive contact interactions. We examine the stability of the PDDWs in the two spontaneous symmetry-breaking branches shown in Fig.1(a) and do find the stable PDDWs. The stable ones are demonstrated by the red-thick lines in the shadow region in Fig.1(a). They only exist in a finite region of  $g$ . When  $g$  is large beyond this region, the interactions obliterate the effect of the SOC, and the system behaves more like the one without the SOC, leading to the PDDWs becoming unstable again.

The similar spontaneous symmetry-breaking behavior of the NBWs shown in Fig.1(a) indicates a similar stability property as the PDDWs. We check the stability of the NBWs in Fig.1(a). The NBWs having spin-flip parity symmetry are always unstable, and there is a region represented by the black-thin lines in the shadow area in the figure where the symmetry-broken NBWs are stable.

The mechanism to stabilize the PDDWs by the SOC is that the SOC makes the parity be associated with the spin-flip, and the contact interactions can break the joint symmetry by spontaneously destroying the spin-flip part to change the effective mass of the PDDWs from originally negative to positive. The stable PDDWs existing in the finite region of  $g$  in Fig. 1(a) stimulate us to search them in the parameter space  $(\Omega, g)$ . We first find the PDDWs for different parameters  $\Omega$  and  $g$ , and then analyze their stability by calculating the BdG equation in Eq. (10). We use the maximum of the imaginary part of  $\omega$ , i.e.,

$$\text{Max}(\text{Im}[\omega]), \quad (12)$$

to show their stability. Only when  $\text{Max}(\text{Im}[\omega]) = 0$ , the corresponding PDDW is stable. The results are demonstrated in Fig. 2(a), where the color scale represents the magnitude of  $\text{Max}(\text{Im}[\omega])$ . In the parameter space  $(\Omega, g)$ , there is a tilted triangle-like region in the middle of the plot (the dark-colored region), inside which most of the PDDWs are stable. The stable PDDWs exist in a finite region of  $\Omega$ . For a fixed  $\Omega$ , the stable region becomes  $g_L < g < g_U$ , with  $g_L$  and  $g_U$  being the lower and upper boundaries of the stable region. The critical values  $g_c$  for the spontaneous symmetry breaking are shown by the open circles in Fig. 2(a). It can be seen that  $g_c < g_L$ , indicating the stable PDDWs break the spin-flip parity symmetry. The existence of  $g_U$  is due to the fact that beyond  $g_U$ , the interactions dominate over the effect of the SOC (including  $\gamma$  and  $\Omega$ ). When  $\Omega$  is small, a small  $g_U$  is needed for the domination, which may lead to  $g_U < g_L$ , giving rise to the vanishing allowable region. Therefore, there is no stable PDDW when  $\Omega$  is small. When  $\Omega$  is large, the Rabi coupling dominates over the SOC in the spin-orbit-coupled Hamiltonian  $H_{SOC}$ , and the system is physically equivalent to a Rabi-coupled two-component BEC without the SOC. In the absence of the SOC, the contact interactions can not break the parity symmetry and consequently can not change the sign of the effective mass of the PDDWs. Therefore, the PDDWs are dynamically unstable when  $\Omega$  is large. Fig. 2(a) shows

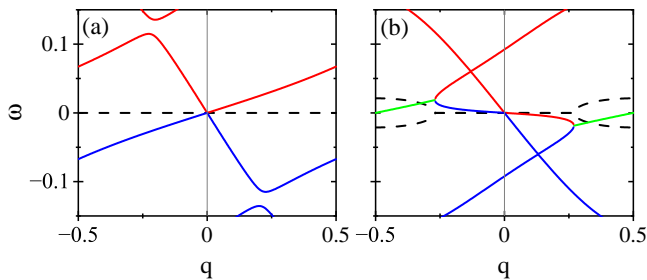


FIG. 3. The Bogoliubov spectrum  $\omega(q)$  of the stable (a) and unstable (b) PDDWs which are labeled by “a” and “b” respectively in Fig. 2(a). (a)  $g = 0.4$  and (b)  $g = 0.24$ . The black-dashed lines are the imaginary part of  $\omega$ , and the red (blue) lines represent the excitations having a positive (negative) Bogoliubov norm  $\mathcal{N}$ . In (b), two excitations with the opposite sign of the norm collide, and after the collision, their real part merges together (the green lines), and the imaginary part appears. The grey vertical lines are for  $q = 0$ , and the other parameters are  $\gamma = 1.95$ ,  $V_0 = 2$  and  $\Omega = 5$ .

that the PDDWs are possibly stable in the region of  $2.7 < \Omega < 5.8$ .

A typical stable (unstable) PDDW is labeled by “a” (“b”) in Fig. 2(a). The Bogoliubov spectrum, i.e., the Bogoliubov eigenvalue  $\omega$  as a function of the quasimomentum of perturbations  $q$ , is demonstrated in Figs. 3(a) and 3(b) respectively for the states “a” and “b”. Considering the  $2\pi$  period of the BdG Hamiltonian for the PDDWs, the Bogoliubov spectrum features the Bloch band-gap structure with the first Brillouin zone  $q \in$

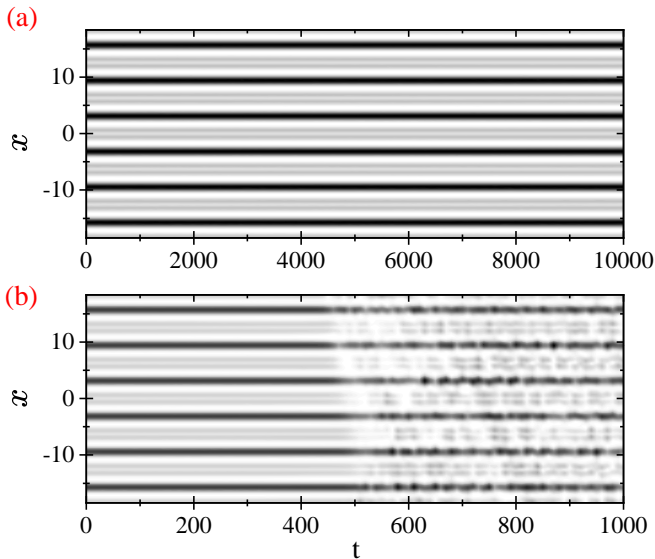


FIG. 4. The nonlinear evolution of the labeled PDDWs “a” and “b” in Fig. 2(a) with a 5% Gaussian distributed random noise. (a) The evolution of the stable state “a”,  $g = 0.4$ . (b) The evolution of the unstable state “b”,  $g = 0.24$ . The other parameters are  $\gamma = 1.95$ ,  $V_0 = 2$  and  $\Omega = 5$ . It is noticed that the time scale is different in (a) and (b).

$(-0.5, 0.5]$ . Only the lowest bands are shown in Fig. 3(a). From the BdG equation in Eq. (10), we define the Bogoliubov norm [67–69],  $\mathcal{N} = \langle \varphi | \tau_z | \varphi \rangle = \int_0^{2\pi} dx (|U_1|^2 + |U_2|^2 - |V_1|^2 - |V_2|^2) / 2\pi$ , with  $\tau_z = \sigma_z \otimes \mathbf{I}$ , and  $\mathbf{I}$  being the  $2 \times 2$  identity matrix. In Fig. 3(a), the excitations in the red lines have  $\mathcal{N} > 0$  and in the blue lines have  $\mathcal{N} < 0$ . The excitation with the negative norm does not have a physical consequence [17]. Therefore, we only consider the positive norm excitations in Fig. 3(a). In the lowest band and  $q \rightarrow 0$ , the spectrum is gapless, which is the signature of the gauge symmetry breaking. The imaginary part of  $\omega$  is always zero, indicating the PDDW “a” is dynamically stable. In contrast, for the PDDW “b”, Fig. 3(b) demonstrates the presence of the imaginary part (the black-dashed lines). Two excitations with opposite signs of the norm  $\mathcal{N}$  collide together, and after the collision, the real part of the two excitations merges, and the imaginary part appears. The sign of the norm is called Krein signature, and the collision of modes with opposite Krein signature can induce the generation of imaginary modes, which is the same as the phenomenon in Fig. 3(b). Such Krein collision physics is attracting research attention in the field of pseudo-Hermitian systems [70, 71].

The stability results shown in Fig. 2(a) can be confirmed by the nonlinear evolution of the PDDWs according to the GPE in Eq. (1). The evolution of the labeled states “a” and “b” in Fig. 2(a) is demonstrated in Figs. 4(a) and 4(b) respectively. For the nonlinear evolution, we incorporate a Gaussian distributed noise with the order of 5% of the initial PDDWs. The “a” state is known to be stable from the linear stability analysis. It can evolve without changing the shape for a very long time in Fig. 4(a). In contrast, the unstable PDDW “b” loses its shape during a short time evolution as shown in Fig. 4(b).

Finally, we also check the stability of the relevant NBWs in the parameter space  $(\Omega, g)$ . The results are demonstrated in Fig. 2(b) with the color scale representing the amplitude of  $\text{Max}(\text{Im}[\omega])$ . The stability of the NBWs has a dramatic difference with the PDDWs in Fig. 2(a). As shown in Fig. 2(b), there are two areas in the parameter space where the NBWs are stable.

## V. CONCLUSION

In this work, we propose to use the SOC to stabilize the PDDWs in BECs with OLs. Without the SOC, these interesting states are always unstable, the reason of which is that their negative effective mass is conserved by the parity symmetry. The SOC makes the parity to be associated with the spin flip, therefore, the joint symmetry becomes the spin-flip parity symmetry. The contact interactions can spontaneously break the spin-flip parity symmetry by destructing the spin-flip channel. The spontaneous symmetry breaking can change the effective mass of the PDDWs from originally negative to positive. With the possibly positive effective mass, the PDDWs

may be dynamically stable. Instructed by this stabilization mechanism, we systematically study the spontaneous symmetry breaking of the PDDWs and check their stability in the full parameter space by analyzing the BdG equations and nonlinear evolutions. We do find the stable PDDWs existing in the experimentally accessible parameter region.

## VI. ACKNOWLEDGE

This work was supported by the National Natural Science Foundation of China (NSFC) with Grants No.

112374247 and No. 11974235, and by the Shanghai Municipal Science and Technology Major Project (Grant No. 2019SHZDZX01-ZX04).

- 
- [1] O. Morsch and M. Oberthaler, Dynamics of Bose-Einstein condensates in optical lattices, *Rev. Mod. Phys.* **78**, 179 (2006).
- [2] I. Bloch, J. Dalibard, and W. Zwerger, Many-body physics with ultracold gases, *Rev. Mod. Phys.* **80**, 3 (2008).
- [3] A. Smerzi, A. Trombettoni, P. G. Kevrekidis, and A. R. Bishop, Dynamical Superfluid-Insulator Transition in a Chain of Weakly Coupled Bose-Einstein Condensates, *Phys. Rev. Lett.* **89**, 170402 (2002).
- [4] B. Wu and Q. Niu, Nonlinear Landau-Zener tunneling, *Phys. Rev. A* **61**, 2, (2000).
- [5] Y. Zhang, Z. Liang, and B. Wu, Gap solitons and Bloch waves in nonlinear periodic systems, *Phys. Rev. A* **80**, 6, (2009).
- [6] S.-L. Zhang, Z.-W. Zhou, and B. Wu, Superfluidity and stability of a Bose-Einstein condensate with periodically modulated interatomic interaction, *Phys. Rev. A* **87**, 013633 (2013).
- [7] R. Dasgupta, B. P. Venkatesh, and G. Watanabe, Attraction-induced dynamical stability of a Bose-Einstein condensate in a nonlinear lattice, *Phys. Rev. A* **93**, 063618 (2016).
- [8] P. J. Y. Louis, E. A. Ostrovskaya, C. M. Savage, and Y. S. Kivshar, Bose-Einstein condensates in optical lattices: Band-gap structure and solitons, *Phys. Rev. A* **67**, 013602 (2003).
- [9] L. Pitaevskii and S. Stringari, Bose-Einstein Condensation and Superfluidity (Oxford University Press, Oxford, UK, 2016).
- [10] Q. Zhu and B. Wu, Superfluidity of Bose-Einstein condensates in ultracold atomic gases, *Chin. Phys. B* **24**, 050507 (2015).
- [11] G. Watanabe, B. Venkatesh, and R. Dasgupta, Nonlinear phenomena of ultracold atomic gases in optical lattices: Emergence of novel features in extended states, *Entropy* **18**, 118 (2016).
- [12] H. He and Y. Zhang, Superfluidity breakdown of Rabi-coupled two-component Bose-Einstein condensates in optical lattices, *Phys. Rev. A* **103**, 053322 (2021).
- [13] J. Hong, C. Wang, and Y. Zhang, Instabilities of a Bose-Einstein condensate with mixed nonlinear and linear lattices, *Phys. Rev. E* **107**, 044219, (2023).
- [14] N. Fabbri, D. Clément, L. Fallani, C. Fort, and M. Modugno, Excitations of Bose-Einstein condensates in a one-dimensional periodic potential, *Phys. Rev. A* **79**, 043623 (2009).
- [15] G. Chauveau, C. Maury, F. Rabec, C. Heintze, G. Brochier, S. Nascimbene, J. Dalibard, J. Beugnon, S. M. Rocuzzo, and S. Stringari, Superfluid Fraction in an Interacting Spatially Modulated Bose-Einstein Condensate, *Phys. Rev. Lett.* **130**, 226003 (2023).
- [16] J. Tao, M. Zhao, and I. B. Spielman, Observation of Anisotropic Superfluid Density in an Artificial Crystal, *Phys. Rev. Lett.* **131**, 163401 (2023).
- [17] B. Wu and Q. Niu, Landau and dynamical instabilities of the superflow of Bose-Einstein condensates in optical lattices, *Phys. Rev. A* **64**, 061603 (2001).
- [18] V. V. Konotop and M. Salerno, Modulational instability in Bose-Einstein condensates in optical lattices, *Phys. Rev. A* **65**, 021602 (2002).
- [19] B. Wu and Q. Niu, Superfluidity of Bose-Einstein condensate in an optical lattice: Landau-Zener tunnelling and dynamical instability, *New J. Phys.* **5**, 104 (2003).
- [20] S. Burger, F. S. Cataliotti, C. Fort, F. Minardi, M. Inguscio, M. L. Chiofalo, and M. P. Tosi, Superfluid and Dissipative Dynamics of a Bose-Einstein Condensate in a Periodic Optical Potential, *Phys. Rev. Lett.* **86**, 4447 (2001).
- [21] L. Fallani, L. De Sarlo, J. E. Lye, M. Modugno, R. Saers, C. Fort, and M. Inguscio, Observation of Dynamical Instability for a Bose-Einstein Condensate in a Moving 1D Optical Lattice, *Phys. Rev. Lett.* **93**, 140406 (2004).
- [22] M. Jona-Lasinio, O. Morsch, M. Cristiani, N. Malossi, J. H. Müller, E. Courtade, M. Anderlini, and E. Arimondo, Asymmetric Landau-Zener Tunneling in a Periodic Potential, *Phys. Rev. Lett.* **91**, 230406 (2003).
- [23] S. B. Koller, E. A. Goldschmidt, R. C. Brown, R. Wyllie, R. M. Wilson, and J. V. Porto, Nonlinear looped band structure of Bose-Einstein condensates in an optical lattice, *Phys. Rev. A* **94**, 063634 (2016).
- [24] J. Liu, L. Fu, B. Ou, S. Chen, D. Choi, B. Wu, and Q. Niu, Theory of nonlinear Landau-Zener tunneling, *Phys. Rev. A* **66**, 023404, (2002).
- [25] Y. Chen, S. D. Huber, S. Trotzky, I. Bloch, and E. Altman, Many-body Landau-Zener dynamics in coupled one-dimensional Bose liquids, *Nature Phys.* **7**, 61-67, (2011).
- [26] Q. Guan, M. K. H. Ome, T. M. Bersano, S. Mossman, P. Engels, and D. Blume, Nonexponential tunneling due

- to mean-field-induced swallowtail, *Phys. Rev. Lett.* **125**, 213401, (2020)
- [27] M. Machholm, A. Nicolin, C. J. Pethick, and H. Smith, Spatial period doubling in Bose-Einstein condensates in an optical lattice, *Phys. Rev. A* **69**, 043604 (2004).
- [28] B. T. Seaman, L. D. Carr, and M. J. Holland, Period doubling, two-color lattices, and the growth of swallowtails in Bose-Einstein condensates, *Phys. Rev. A* **72**, 033602 (2005).
- [29] B.-G. Yang, P.-J. Tang, X.-X. Guo, X.-Z. Chen, B. Wu, and X.-J. Zhou, Period-Doubled Bloch States in a Bose-Einstein Condensate, *Chin. Phys. Lett.* **35**, 070301 (2018).
- [30] S. Yoon, F. Dalfovo, T. Nakatsukasa, and G. Watanabe, Multiple period states of the superfluid Fermi gas in an optical lattice, *New J. Phys.* **18** 023011 (2016).
- [31] A. Maluckov, G. Gligorić, and L. Hadžievski, B. A. Malomed, and T. Pfau, Stable Periodic Density Waves in Dipolar Bose-Einstein Condensates Trapped in Optical Lattices, *Phys. Rev. Lett.* **108**, 140402 (2012).
- [32] Y. K. Kato, R. C. Myers, A. C. Gossard, and D. D. Awschalom, Observation of the spin Hall effect in semiconductors, *science* **306**, 1910 (2004).
- [33] B. A. Bernevig and S.-C. Zhang, Quantum Spin Hall Effect, *Phys. Rev. Lett.* **96**, 106802 (2006).
- [34] Y.-J. Lin, K. Jiménez-García, and I. B. Spielman, Spin-orbit-coupled Bose-Einstein condensates, *Nature* **471**, 83 (2011).
- [35] L. W. Cheuk, A. T. Sommer, Z. Hadzibabic, T. Yefsah, W. S. Bakr, and M. W. Zwierlein, Spin-injection spectroscopy of a spin-orbit coupled Fermi gas, *Phys. Rev. Lett.* **109**, 095302 (2012).
- [36] P. Wang, Z.-Q. Yu, Z. Fu, J. Miao, L. Huang, S. Chai, H. Zhai, and J. Zhang, Spin-orbit coupled degenerate Fermi gases, *Phys. Rev. Lett.* **109**, 095301 (2012).
- [37] M. A. Khamsehchi, Y. Zhang, C. Hamner, T. Busch, and P. Engels, Measurement of collective excitations in a spin-orbit-coupled Bose-Einstein condensate, *Phys. Rev. A* **90**, 063624 (2014).
- [38] S.-C. Ji, L. Zhang, X.-T. Xu, Z. Wu, Y. Deng, S. Chen, and J.-W. Pan, Softening of roton and phonon modes in a Bose-Einstein condensate with spin-orbit coupling, *Phys. Rev. Lett.* **114**, 105301 (2015).
- [39] C. Hamner, Y. Zhang, M. A. Khamsehchi, M. J. Davis, and P. Engels, Spin-Orbit-Coupled Bose-Einstein Condensates in a One-Dimensional Optical Lattice, *Phys. Rev. Lett.* **114**, 070401 (2015).
- [40] Z. Wu, L. Zhang, W. Sun, X.-T. Xu, B.-Z. Wang, S.-C. Ji, Y. Deng, S. Chen, X.-J. Liu, and J.-W. Pan, Realization of two-dimensional spin-orbit coupling for Bose-Einstein condensates, *Science* **354**, 83 (2016).
- [41] J. Li, J. Lee, W. Huang, S. Burchesky, B. Shteynas, F. Ç. Top, A. O. Jamison, and W. Ketterle, A stripe phase with supersolid properties in spin-orbit-coupled Bose-Einstein condensates, *Nature* **543**, 91–94 (2017).
- [42] C. Wang, C. Gao, C.-M. Jian, and H. Zhai, Spin-Orbit Coupled Spinor Bose-Einstein Condensates, *Phys. Rev. Lett.* **105**, 160403 (2010).
- [43] T.-L. Ho and S. Zhang, Bose-Einstein condensates with spin-orbit interaction, *Phys. Rev. Lett.* **107**, 150403 (2011).
- [44] H. Hu, B. Ramachandhran, H. Pu, and X.-J. Liu, Spin-orbit coupled weakly interacting Bose-Einstein condensates in harmonic traps, *Phys. Rev. Lett.* **108**, 010402 (2012).
- [45] Y. Li, G. I. Martone, L. P. Pitaevskii, and S. Stringari, Superstripes, and the excitation spectrum of a spin-orbit-coupled Bose-Einstein condensate, *Phys. Rev. Lett.* **110**, 235302 (2013).
- [46] W. Zheng, Z.-Q. Yu, X. Cui, and H. Zhai, Properties of Bose gases with the Raman-induced spin-orbit coupling, *J. Phys. B: At. Mol. Opt. Phys.* **46**, 134007 (2013).
- [47] Y. Zhang, M. E. Mossman, T. Busch, P. Engels, and C. Zhang, Properties of spin-orbit-coupled Bose-Einstein condensates, *Front. Phys.* **11**, 118103 (2016).
- [48] T. M. Bersano, J. Hou, S. Mossman, V. Gokhroo, X. Luo, K. Sun, C. Zhang, and P. Engels, Experimental realization of a long-lived striped Bose-Einstein condensate induced by momentum-space hopping, *Phys. Rev. A* **99**, 051602(R) (2019).
- [49] Y. V. Kartashov, V. V. Konotop, D. A. Zezyulin, and L. Torner, Bloch Oscillations in Optical and Zeeman Lattices in the Presence of Spin-Orbit Coupling, *Phys. Rev. Lett.* **117**, 215301 (2016).
- [50] Z. Cai, X. Zhou, and C. Wu, Magnetic phases of bosons with synthetic spin-orbit coupling in optical lattices, *Phys. Rev. A* **85**, 061605 (2012).
- [51] W. S. Cole, S. Zhang, A. Paramekanti, and N. Trivedi, Bose-Hubbard Models with Synthetic Spin-Orbit Coupling: Mott Insulators, Spin Textures, and Superfluidity, *Phys. Rev. Lett.* **109**, 085302 (2012).
- [52] J. Radić, A. Di Ciolo, K. Sun, and V. Galitski, Exotic Quantum Spin Models in Spin-Orbit-Coupled Mott Insulators, *Phys. Rev. Lett.* **109**, 085303 (2012).
- [53] Z. Chen and Z. Liang, Ground-state phase diagram of a spin-orbit-coupled bosonic superfluid in an optical lattice, *Phys. Rev. A* **93**, 013601 (2016).
- [54] G. I. Martone, T. Ozawa, C. Qu, and S. Stringari, Optical-lattice-assisted magnetic phase transition in a spin-orbit-coupled Bose-Einstein condensate, *Phys. Rev. A* **94**, 043629 (2016).
- [55] W. Ji, K. Zhang, W. Zhang, and L. Zhou, Bloch oscillations of spin-orbit-coupled cold atoms in an optical lattice and spin-current generation, *Phys. Rev. A* **99**, 023604 (2019).
- [56] X. Luo, Z. Hu, Z.-Y. Zeng, Y. Luo, B. Yang, J. Xiao, L. Li, and A.-X. Chen, Analytical results for the superflow of spin-orbit-coupled Bose-Einstein condensates in optical lattices, *Phys. Rev. A* **103**, 063324 (2021).
- [57] G. Li, X. Luo, J. Hou, and C. Zhang, Pseudo-Goldstone excitations in a striped Bose-Einstein condensate, *Phys. Rev. A* **104**, 023311.
- [58] D. A. Zezyulin and V. V. Konotop, Localization of ultracold atoms in Zeeman lattices with incommensurate spin-orbit coupling, *Phys. Rev. A* **105**, 063323 (2022).
- [59] J. Yang and Y. Zhang, Spin-orbit-coupled spinor gap solitons in Bose-Einstein condensates, *Phys. Rev. A* **107**, 023316, (2023).
- [60] Y. Zhang and C. Zhang, Bose-Einstein condensates in spin-orbit-coupled optical lattices: Flat bands and superfluidity, *Phys. Rev. A* **87**, 023611 (2013).
- [61] C. Wang, Y. Zhang, and V. V. Konotop, Wannier solitons in spin-orbit-coupled Bose-Einstein condensates in optical lattices with a flat band, *Phys. Rev. A* **108**, 013307 (2023).
- [62] S. Mardonov, M. Modugno, and E. Y. Sherman, Dynamics of spin-orbit coupled Bose-Einstein condensates in a random potential, *Phys. Rev. Lett.* **115**, 180402 (2015).



- [63] S. Mardonov, V. V. Konotop, B. A. Malomed, M. Modugno, and E. Y. Sherman, Spin-orbit-coupled soliton in a random potential, *Phys. Rev. A* **98**, 023604 (2018).
- [64] M. Machholm, C. J. Pethick, and H. Smith, Band structure, elementary excitations, and stability of a Bose-Einstein condensate in a periodic potential, *Phys. Rev. A* **67**, 053613 (2003).
- [65] I. Danshita and S. Tsuchiya, Stability of Bose-Einstein condensates in a Kronig-Penney potential, *Phys. Rev. A* **75**, 033612 (2007).
- [66] T. Ozawa, L. P. Pitaevskii, and S. Stringari, Supercurrent and dynamical instability of spin-orbit-coupled ultracold Bose gases, *Phys. Rev. A* **87**, 063610 (2013).
- [67] D. V. Skryabin, Instabilities of vortices in a binary mixture of trapped Bose-Einstein condensates: Role of collective excitations with positive and negative energies, *Phys. Rev. A* **63**, 013602 (2000).
- [68] Y. Kawaguchi and T. Ohmi, Splitting instability of a multiply charged vortex in a Bose-Einstein condensate, *Phys. Rev. A* **70**, 043610 (2004).
- [69] E. Lundh and H. M. Nilsen, Dynamic stability of a doubly quantized vortex in a three-dimensional condensate, *Phys. Rev. A* **74**, 063620 (2006).
- [70] A. Melkani, Degeneracies and symmetry breaking in pseudo-Hermitian matrices, *Phys. Rev. Research* **5**, 023035 (2023).
- [71] G. A. Starkov, M. V. Fistul, and I. M. Eremin, Formation of exceptional points in pseudo-Hermitian systems, *Ann. Phys.* **456**, 169268 (2023).